Hybrid Molecular-Based Magnets Containing Organic NLO Chromophores: A Search toward an Interplay between Magnetic and NLO Behavior

Pascal G. Lacroix* and Isabelle Malfant

Laboratoire de Chimie de Coordination du CNRS, 205 route de Narbonne, 31077 Toulouse, France

Sophie Bénard, Pei Yu,* and Eric Rivière

Laboratoire de Chimie Inorganique, URA 420, Université Paris-Sud, 91405 Orsay, France

Keitaro Nakatani

PPSM, Ecole Normale Supérieure de Cachan, URA 1906, Avenue du Pdt Wilson, 94235 Cachan, France

Received September 22, 2000

A new hybrid molecular-based ferromagnet of formula $[(dmaph)PPh_3][MnCr(ox)_3]$, where $[(dmaph)PPh_3]^+$ stands for the (4-dimethylaminophenyl)triphenylphosphonium cation (ox^{2-} being the oxalate anion), has been synthesized. It crystallizes in the monoclinic $P2_1$ space group, with lattice parameters $a = 13.954(2)$ Å, $b = 16.297(2)$ Å, $c = 14.323(2)$ Å, and $\beta = 99.27(1)°$. Refinement based on F_o^2 yields $R = 0.072$ and $wR_2 = 0.156$. The compound exhibits a ferromagnetic interaction between Cr^{3+} and Mn^{2+}, with a long-range magnetic ordering at $T_C = 4.5$ K. The hyperpolarizability (β) of the cation is calculated within the framework of the INDO/SOS-based method, which indicates a β value comparable to that of *p*-nitroaniline for an absorption maximum at 306 nm ($\epsilon_{max} = 28\ 500\ M^{-1}\ cm^{-1}$). This result is consistent with the observation of a SHG efficiency 4 times that of urea for the parent $[(dmaph)PPh_3]Br$ salt, at 1.907 μm. The non-centrosymmetric $[(dmaph)PPh_3][Mn^{II}Cr^{III}(ox)_3]$ derivative is used as a model compound for an investigation of the potential effect of a ferromagnetic ordering on the bulk NLO response of hybrid materials made of NLO cations inserted between magnetic anionic layers.

Introduction

Molecular materials have emerged in many areas of material science for designing new magnets,[1] molecular assemblies for data storage,[2] materials for nonlinear optics,[3,4] and conductors and superconductors.[5,6] The versatility of molecular chemistry offers a unique opportunity to meet additional challenges, such as designing multiproperty materials that would simultaneously possess several properties (e.g., magnetism and conductivity,[7,8] magnetism and nonlinear optical (NLO) properties,[9−11] or conductivity and NLO properties[12,13]). In such materials, the possibility for interplay between the properties is naturally addressed and could attract much interest in connection with the development of molecular swiches.[14,15]

Along this line, we have previously reported on several magnetic anionic structures with NLO cations inserted in between, in particular $Mn_{0.86}P_2S_6(DAMS)_{0.28}$

(1) (a) Kahn, O. *Molecular Magnetism*; VCH: Weinheim, 1993. (b) Miller, J. S.; Epstein, A. J. *Angew. Chem., Int. Ed. Engl.* **1994**, *33*, 385.
(2) Kahn, O.; Martinez, C. J. *Science* **1998**, *279*, 44.
(3) Optical Nonlinearities in Chemistry; special issue of *Chem. Rev.* **1994**, *94* (1).
(4) (a) Zyss, J. *Molecular Nonlinear Optics: Materials, Physics and Devices*; Academic Press: Boston, 1994. (b) *Nonlinear Optics of Organic Molecules and Polymers*; Nalwa, H. S., Miyata, S., Eds.; CRC Press: New York, 1997.
(5) *J. Mater. Chem.* Special Issue on Molecular Conductors **1995**, *5* (10).
(6) (a) Cassoux, P.; Miller, J. S. In *Chemistry of Advanced Materials: An Overview*; Interrante, L. V., Hampden-Smith, M. J., Eds.; Wiley-VCH: New York, 1998; p 19. (b) Williams, J. M.; Ferraro, J. R.; Thorn, R. J.; Carlson, K. D.; Geiser, U.; Wang, H. H.; Kini, A. M.; Whangbo, M. H. *Organic Superconductors (Including Fullerenes)*; Prentice Hall: Englewood Cliffs, NJ, 1992.
(7) Goze, F.; Laukhin, V. N.; Brossard, L.; Audouard, A.; Ulmet, J. P.; Askenazy, S.; Naito, T.; Kobayashi, H.; Kobayashi M.; Cassoux, P. *Europhys. Lett.* **1994**, *28*, 427.
(8) Kurmoo, M.; Graham, A. W.; Day, P.; Coles, S. J.; Hursthouse, M. B.; Caulfield, J. L.; Singleton, J.; Pratt, F. L.; Hayes, W.; Ducasse L.; Guionneau, P. *J. Am. Chem. Soc.* **1995**, *117*, 12209.
(9) (a) Clément, R.; Lacroix, P. G.; O'Hare D.; Evans, J. *Adv. Mater.* **1994**, *6*, 794. (b) Lacroix, P. G.; Clément, R.; Nakatani, K.; Zyss J.; Ledoux, I. *Science* **1994**, *263*, 658.
(10) Bernard, S.; Yu, P.; Coradin, T.; Rivière, E.; Nakatani, K.; Clément, R. *Adv. Mater.* **1997**, *9*, 981.
(11) Averseng, F.; Lepetit, C.; Lacroix, P. G.; Tuchagues, J.-P. *Chem. Mater.* **2000**, *12*, 2225.
(12) Sutter, K.; Hulliger J.; Günter, P. *Solid State Commun.* **1990**, *74*, 867.
(13) (a) Lacroix P. G.; Nakatani, K. *Adv. Mater.* **1997**, *9*, 1105. (b) Malfant, I.; Cordente, N.; Lacroix, P. G.; Lepetit, C. *Chem. Mater.* **1998**, *10*, 4079.
(14) Lehn, J.-M. *Supramolecular Chemistry: Concepts and Perspectives*; VCH: Weinheim, 1995.
(15) Ward, M. D. *Chem. Soc. Rev.* **1995**, *24*, 121.

10.1021/cm001177v CCC: $20.00
Published on Web 01/27/2001

Scheme 1

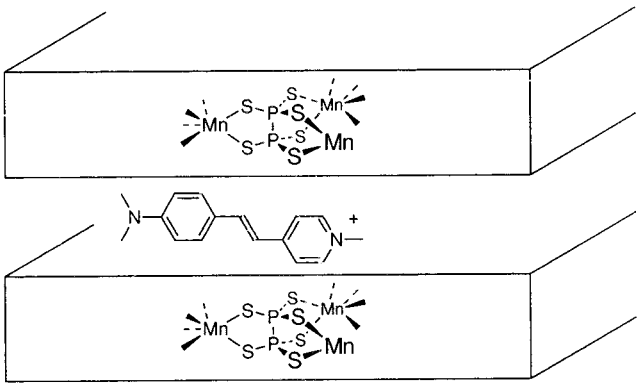

$Mn_{0.86}PS_3(DAMS)_{0.28}$ **(1)**

Curie temperature	SHG
40 K	300 × urea

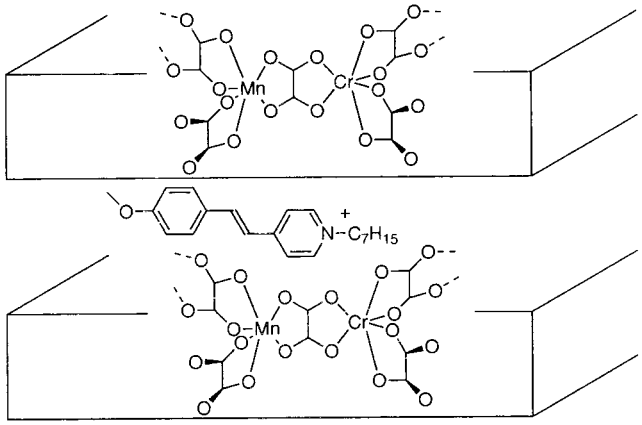

$[(MHS)[Mn^{II}Cr^{III}(ox)_3]$ **(2)**

Curie temperature	SHG
5.7 K	100 × urea

(Scheme 1, compound **1**), in which 4′-(dimethylamino)-*N*-methystilbazolium ($DAMS^+$) cations have been intercalated into $Mn_2P_2S_6$ lamellar materials,[9] and (MHS)-$[Mn^{II}Cr^{III}(ox)_3]$ (Scheme 1, compound **2**), in which 4′-methoxy-*N*-heptylstilbazolium $(MHS)^+$ cations are inserted between $[Mn^{II}Cr^{III}(ox)_3]^-$ anionic layers.[10] Both hybrid materials combine a large efficiency in second-harmonic generation (SHG) and a permanent magnetization at low temperature. However, the structure−property relationships were not established in either case because of a lack of suitable crystal structure, and hence no rationale for a possible interplay has been suggested between the properties.

In the present contribution, we wish to report on the first crystal structure of a non-centrosymmetric ferromagnet containing NLO chromophores, $[(dmaph)PPh_3]$-$[Mn^{II}Cr^{III}(ox)_3]$, in which ($[(dmaph)PPh_3]^+$ is the (4-dimethylaminophenyl)triphenylphosphonium cation and $(ox)^{2-}$ the oxalate anion). The magnetic properties are thoroughly investigated in the first section. Then, the molecular NLO response (β) of the cations is discussed within the chemically oriented INDO−SOS formalism. Although the structure is non-centrosymmetric, no SHG efficiency is observed because of pseudo-centrosymmetric packing of the cations in solid state. Nevertheless, $[(dmaph)PPh_3][Mn^{II}Cr^{III}(ox)_3]$ is used as a model compound for evaluating the potential effect of the Faraday rotation occurring upon magnetic transition on the NLO response of such hybrid lamellar magnets.

Experimental Section

Starting Materials and Equipment. 4-Bromo-*N*,*N*-dimethylaniline, triphenyl phosphine, and palladium(II) acetate were purchased from Acros Organics and $Mn(NO_3)_2{\cdot}4H_2O$ from Fluka. All of them were used without further purification. $K_3[Cr(ox)_3]{\cdot}3H_2O$ was synthesized by following a literature procedure.[16] ^1H NMR spectra were recorded on a 250-MHz Bruker spectrometer and electronic spectra on a Varian Cary 5E spectrophotometer. Elemental analyses were performed by the Service de Microanalyse du CNRS in Gif sur Yvette. The magnetic studies were carried out on a Quantum Design SQUID magnetometer working in dc mode. The diamagnetic correction was estimated equal to -3.76×10^{-4} cm^3 mol^{-1}. The magnetic field was 0.05 and 0.003 T for the susceptibility and magnetization measurements, respectively. Because of very weak hysteresis, no coercive field was measured. The SHG intensities were recorded by the Kurtz-Perry powder technique,[17] using a nanosecond Nd:YAG pulsed (10 Hz) laser on microcrystalline powder samples obtained by grinding and put between two glass plates.

Syntheses. *[(dmaph)PPh$_3$]Br*. Following a general route previously reported,[18] a mixture of 1 g (5 mmol) of 4-bromo-*N*,*N*-dimethylaniline, 1.3 g (5 mmol) of triphenylphosphine, and 11 mg (0.05 mmol) of palladium acetate in ≈8 mL of *p*-xylene was refluxed overnight, and the resulting white microcrystalline solid was filtered out, washed with *p*-xylene, and dried under vacuum (yield: 48%). ^1H NMR (CD_3OD): δ

(16) *Handbook of Preparative Inorganic Chemistry*; Brauer, G., Ed; Academic Press: New York-London, 1965; p 1372.

(17) (a) Kurtz, S. K.; Perry, T. T. *J. Appl. Phys.* **1968**, *39*, 3798. (b) Dougherty, J. P.; Kurtz, S. K. *J. Appl. Crystallogr.* **1976**, *9*, 145.

(18) Migita, T.; Nagai, T.; Kiuchi, K.; Kosugi, M. *Bull. Chem. Soc. Jpn.* **1983**, *56*, 2869.

Table 1. Crystallographic Data for [(dmaph)PPh_3][$Mn^{II}Cr^{III}(ox)_3^-$]

chemical formula	$C_{64}H_{50}Cr_2Mn_2N_2O_{124}P_2$
fw (g mol^{-1})	1506.88
size (mm)	0.25 × 0.25 × 0.125
crystal system	monoclinic
space group	$P2_1$
a (Å)	13.954(2)
b (Å)	16.297(2)
c (Å)	14.303(2)
β (deg)	99.27(1)
V (Å^3)	3211.52
Z	2
D_{calc}	1.558
F(000)	1536.0
μ(Mo Kα) (cm^{-1})	8.193
temperature (K)	160
scan mode	ϕ
scan range ϕ, deg	$0 < \phi < 250.5$
2θ range, deg	$2.9 < \theta < 48.4$
reflections collected	26 116
independent reflections	10 154
range of h, k, l	$-16 \le h \le 16$
	$-18 \le k \le 18$
	$-16 \le l \le 16$
refinement on	F^2
R^a (for $F > 2(F)$)	0.0720
$wR_2{}^b$	0.1563
no. of variables	870
$\Delta\rho_{max}$, e Å^{-3}	0.356
$\Delta\rho_{min}$, e Å^{-3}	−0.580
GOF	0.868

[a] $R = \Sigma(||F_o| - |F_c||)/\Sigma(|F_o|)$ and $wR_2 = \Sigma(w(F_o^2 - F_c^2)^2/\Sigma w(F_o^2)^2]^{1/2}$.

3.13 (s, 6H), 6.98 (dd, 9.1, 2.8 Hz, 2H), 7.38 (d, 9.1 Hz, 1H), 7.45 (d, 9.1 Hz, 1H), 7.65−7.95 (m, 15H). Anal. Calcd (found) for $C_{26}H_{25}BrNP\cdot H_2O$: C, 65.01 (64.91); H, 5.67 (5.44); N, 2.92 (3.02).

[(dmaph)PPh_3][$Mn^{II}Cr^{III}(ox)_3$]. A mixture of 96 mg (0.2 mmol) of [(dmaph)PPh_3]Br and 97 mg (0.2 mmol) of K_3[$Cr(ox)_3$]·3 H_2O was dissolved in a mixture of 4 mL of MeOH and 4 mL of water. To the resulting solution was added 50 mg (0.2 mmol) of $Mn(NO_3)_2\cdot 4H_2O$ dissolved in a small amount of MeOH. A pale green polycrystalline solid was filtered, successively washed with a mixture of MeOH−H_2O, H_2O, MeOH, and finally dyed under vacuum (yield: 67%). Anal. Calcd (found) for $C_{32}H_{26}CrMnNO_{12}P$: C, 50.94 (50.63); H, 3.47 (3.41); N, 1.86 (1.85). Single crystals suitable for X-ray structure determination were obtained as follows: in one arm of a H-shaped tube, a MeOH/H_2O (1/2) solution of 0.1 mmol of $MnNO_3\cdot 4H_2O$ was slowly diffused into a solution containing 0.1 mmol of [(dmaph)PPh_3]Br and 0.1 mmol of K_3[$Cr(ox)_3$]·$3H_2O$ in the other arm of the tuble. Large diamond-shaped crystals were obtained over a period of 2 months.

X-ray Crystallography. The data were collected at 160 K on a Stoe Imaging Plate Diffraction System (IPDS) equipped with an Oxford Cryosystems cooler device, with a tube power of 1.8 kW (50 kV, 36 mA). The crystal-to-detector distance was 80 mm; 167 exposures (6 min/exposure) were obtained with $0° < \varphi < 250.5°$ and with the crystals rotated through 1.5° in φ. Numerical absorption corrections were considered, with $T_{min} = 0.804$ and $T_{max} = 0.900$.

The structure was solved by direct methods (Shelxs-97),[19] and 870 parameters using 488 restraints were refined using the least-squares procedures on F^2.[20] Hydrogen atoms were introduced in the calculation in idealized positions (d(C−H) = 0.99 Å) and their atomic coordinates were recalculated after each cycle. They were given isotropic thermal parameters 20% higher than those of the carbon to which they are attached. Least-squares refinements were carried out by minimizing the function wR_2. Criteria for a satisfactory complete analysis were the ratios of the root-mean-squared shift to standard deviation less than 0.1 and no significant features in final difference maps. Details of data collection and refinement are given in Table 1. The drawing of the molecule was realized with the help of CAMERON.[21]

Table 2. Metal−Oxygen Bond Lengths (Å) in [(dmaph)PPh_3][$Mn^{II}Cr^{III}(ox)_3$] versus Those of Previously Reported [A][$Mn^{II}Cr^{III}(ox)_3$]Crystal Structures

[A]$^+$ = [(dmaph)PPh_3]$^+$			
Mn(1)−O(6)	2.037(18)	Cr(1)−O(1)	2.004(18)
Mn(1)−O(8)	2.048(15)	Cr(1)−O(14)	2.020(18)
Mn(1)−O(5)	2.053(16)	Cr(1)−O(12)	2.073(13)
Mn(1)−O(7)	2.066(15)	Cr(1)−O(2)	2.070(15)
Mn(1)−O(4)	2.127(16)	Cr(1)−O(15)	2.088(17)
Mn(1)−O(3)	2.150(16)	Cr(1)−O(13)	2.138(16)
Mn(2)−O(16)	2.009(19)	Cr(2)−O(11)	1.986(16)
Mn(2)−O(18)	2.017(14)	Cr(2)−O(19)(*i*)	1.997(19)
Mn(2)−O(20)	2.071(18)	Cr(2)−O(22)(*ii*)	2.075(19)
Mn(2)−O(24)	2.078(16)	Cr(2)−O(10)	2.081(18)
Mn(2)−O(21)	2.089(16)	Cr(2)−O(9)	2.094(18)
Mn(2)−O(17)	2.115(18)	Cr(2)−O(23)(*ii*)	2.096(17)

symmetry transformations used to generate equivalent atoms: (*i*) $x, y + 1, z$; (*ii*) $-x, y + 1/2, -z$

[A]$^+$ =	$[NBu_4]^+$ [a]	$[PPh_4]^+$ [b]	$[NPr_4]^+$ [c]	$[NPrBu_3]^+$ [c]	$[PBuPh_3]^+$ [c]
Mn−O	2.14(2)	2.13(2)	2.19(1)	2.212(9)	2.11(1)
	2.15(2)		2.14(2)	2.133(9)	2.06(1)
Cr−O	1.97(2)	2.02(2)	2.03(1)	1.98(1)	2.05(2)
	2.03(2)		1.92(1)	1.935(9)	2.08(2)

[a] Reference 22. [b] Reference 23. [c] Reference 21.

By contrast versus the *R*3*c* space group previously reported for most honeycomb bimetallic oxalato-bridged networks,[22−26] cell parameters and extinction lead to the monoclinic $P2_1/n$ space group. The major consequence is a break in the alternate ...−Cr−Mn−... hexagonal ring, with the appearance of Mn−Mn and Cr−Cr linkages arising from symmetry operations dictated by $P2_1/n$ (inversion center). However, the magnetic data do not reflect these structural features (vide infra). In addition, it is well-known that tetraarylphosphonium salts usually crystallize in non-centrosymmetric space groups.[27] Consequently, the present crystallographic data probably result from racemic twins (twin by inversion). This explanation is strongly supported by the value of the metal−oxygen distances, compared with those of previously reported [Mn^{II}-$Cr^{III}(ox)_3$]$^-$-based crystal structures.[22−24] In most cases, the Mn^{II} and Cr^{III} ions can be distinguished from a comparison of the metal−oxygen interatomic distances. By contrast, Mn^{II} and Cr^{III} cannot be discriminated on the basis of metal−oxygen bond lengths in [(dmaph)PPh_3][$Mn^{II}Cr^{III}(ox)_3$]. This situation previously encountered for [$PBuPh_3$][$Mn^{II}Cr^{III}(ox)_3$] was analyzed as arising from a twin structure obtained by interchanging the position of Mn^{II} and Cr^{III} upon passing from one layer to another one.[22] Therefore, to account for the magnetic properties of [(dmaph)PPh_3][$Mn^{II}Cr^{III}(ox)_3$], the possibility to ascribe the present crystal data in the non-centrosymmetric $P2_1$ space group was considered, through a treatment of the inversion twins using the tools available in Shelxs-97, with a fractionnal contribution of 0.51(8), which assumes that roughly

(19) Sheldrick, G. M. *Acta Crystallogr.* **1990**, *A46*, 467.
(20) Sheldrick, G. M. *SHELXS97, Program for Crystal Structure Solution*; University of Göttingen: Göttingen, Germany, 1986.
(21) Watkin, D. J.; Prout, C. K.; Pearce, L. J. *CAMERON*; Chemical Crystallography Laboratory, University of Oxford: Oxford, 1996.
(22) Shilov, G. V.; Atovmyan, L. O.; Ovanesyan, N. S.; Pyalling, A. A.; Bottyan, L. *Russ. J. Coord. Chem.* **1998**, *24*, 288.
(23) Atovmyan, L. O.; Shilov, G. V.; Lyubovskaya, R. N.; Zhilyaeva, E. I.; Ovanesyan, N. S.; Pirumova, S. I.; Gusakovskaya, I. G.; Morozov, Y. G. *JETP Lett.* **1993**, *10*, 766.
(24) Decurtins, S.; Schmalle, H. W.; Oswald, H. R.; Linden, A.; Ensling, J.; Gütlich, P.; Hauser, A. *Inorg. Chim. Acta* **1994**, *216*, 65.
(25) Mathonière, C.; Nuttall, C. J.; Carling, S. G.; Day, P. *Inorg. Chem.* **1996**, *35*, 1201.
(26) Pellaux, R.; Schmalle, H. W.; Huber, R.; Fischer, P.; Hauss, T.; Ouladdiaf, B.; Decurtins, S. *Inorg. Chem.* **1997**, *36*, 2301.
(27) (a) Lloyd, M. A.; Pratt Brock, C. *Acta Crystallogr. B* **1997**, *53*, 773 (b) Lloyd, M. A.; Pratt Brock, C. *Acta Crystallogr. B* **1997**, *53*, 780.

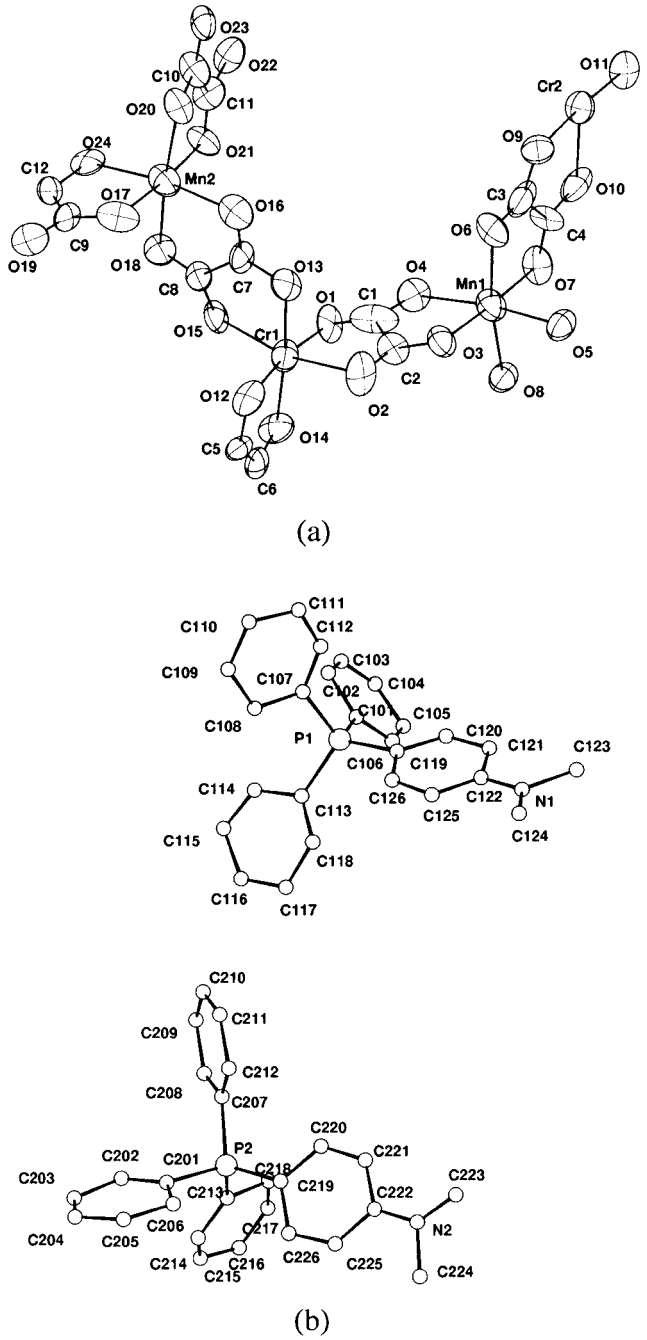

Figure 1. CAMERON view and atom labeling of $[Mn^{II}Cr^{III}(ox)_3]^-$ anions (a) and $[(dmaph)PPh_3]^+$ cations (b), with cation **1** (**2**) being on the top (bottom).

one-half of the layers exhibit $-[Mn^{II}-Cr^{III}]-$ alternation and one-half $-[Cr^{III}-Mn^{II}]-$ alternation. This leads to satisfactory agreement from both crystallographic and magnetic points of view.

The metal−oxygen bond lengths of $[(dmaph)PPh_3][Mn^{II}Cr^{III}(ox)_3]$ are summarized in Table 2 for a comparison with the previously reported $[Mn^{II}Cr^{III}(ox)_3]^-$-based crystal structures. The mean Mn−O and Cr−O distances are equal to 2.072 and 2.060 Å, respectively. Full interatomic distances and bond angles, fractional atomic coordinates, and the equivalent thermal parameters for all atoms and anisotropic thermal parameters for non-hydrogen atoms have been deposited at the Cambridge Crystallographic Data Center.

Semiempirical Computations. The INDO/1 (intermediate neglect of differential overlap)[28] method, in connection with the sum-over-state (SOS) formalism,[29] was employed for the calculation of the molecular hyperpolarizability of $[(dmaph)PPh_3]^+$ cation, using the commercially available CAChe work system (Oxford Molecular). Details of the computationally efficient INDO−SOS-based method for describing second-order molecular optical nonlinearities have been reported elsewhere.[30] The monoexcited configuration interaction (MECI) approximation was employed to describe the excited states. The 100 energy transitions between the 10 highest occupied molecular orbitals and the 10 lowest unoccupied ones were chosen to undergo configuration interaction (CI) mixing. Structural parameters used for the calculations were taken from the present crystal structure (cation 1).

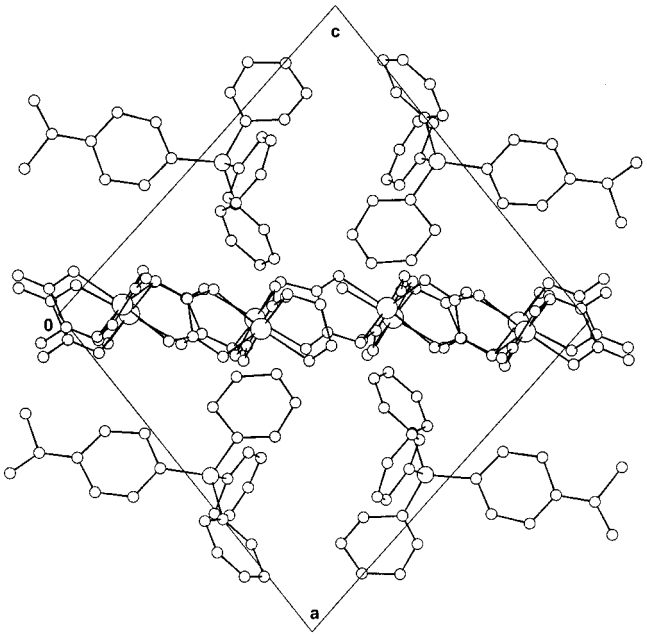

Figure 2. Crystal structure for $[(dmaph)PPh_3][Mn^{II}Cr^{III}(ox)_3]$ showing the NLO cations inserted between the $[Mn^{II}Cr^{III}(ox)_3]^-$ layers.

Results and Discussion

Crystal Structure of $[(dmaph)PPh_3][MnCr(ox)_3]$. The asymmetric unit cell contains one anion made of two Mn^{II}, two Cr^{III}, six oxalate ligands (Figure 1a), and two $[(dmaph)PPh_4]^+$ cations (Figure 1b). The structure (Figure 2) consists of anionic layers of the honeycomb bimetallic $Mn^{II}Cr^{III}$ oxalato-bridged networks with (4-dimethylaminophenyl)triphenylphosphonium cations intercalated in between. The interlayer distance (10.864 Å) is higher than what has been observed in related $(NR_4)[MnCr(ox)_3]$ and $(PR_4)[MnCr(ox)_3]$ derivatives.[22−24] Cations and anions are well separated, by contrast with the previous structures in which the cations point vertically to the anionic layers. Projection of one layer onto the $(10\bar{1})$ plane is shown in Figure 3. The two cations present in the asymmetric unit cell are fairly well aligned with an angle between the two charge transfer (N(1)−P(1) and N(2)−P(2) direction) axes equal to 6.26°. However, the presence of a 2_1 helicoidal axis gives rise to pseudo-centrosymmetric crystal environment, which should lead to almost vanishing NLO properties in the solid state (vide infra).

(28) (a) Zerner, M.; Loew, G.; Kirchner, R.; Mueller-Westerhoff, U. *J. Am. Chem. Soc.* **1980**, *102*, 589. (b) Anderson, W. P.; Edwards, D; Zerner, M. C. *Inorg. Chem.* **1986**, *25*, 2728.
(29) Ward, J. F. *Rev. Mod. Phys.* **1965**, *37*, 1.
(30) Kanis, D. R.; Ratner, M. A.; Marks, T. J. *Chem. Rev.* **1994**, *94*, 195.

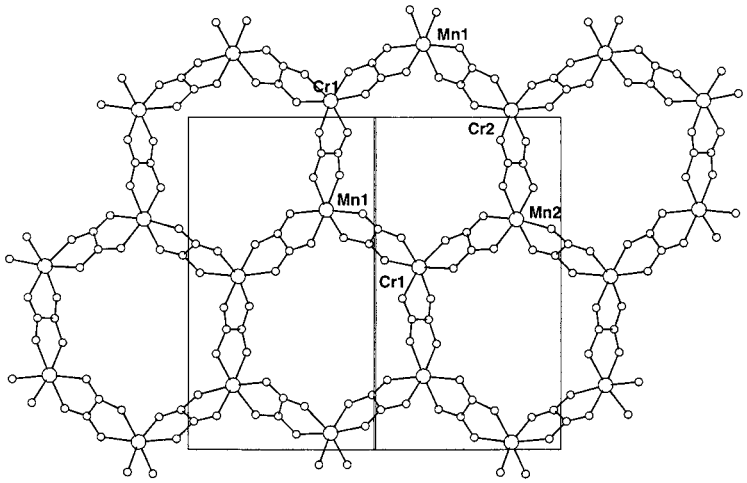

Figure 3. Projection of the crystal structure onto the $(10\bar{1})$ plane.

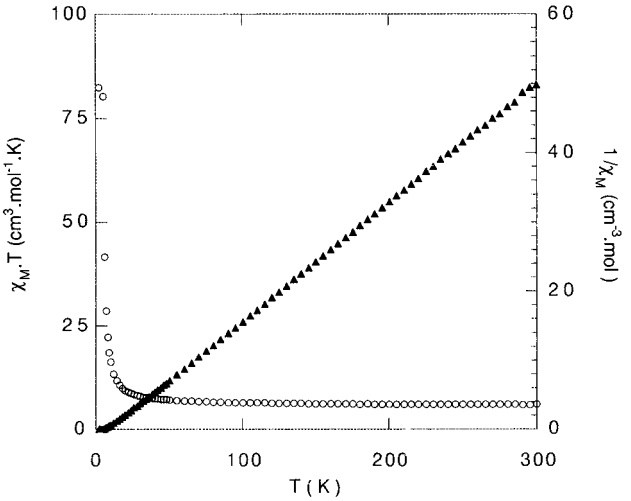

Figure 4. Temperature dependence of $\chi_M \times T$ (white circle) and $1/\chi_M$ (black triangle) for $[(dmaph)PPh_3][Mn^{II}Cr^{III}(ox)_3]$.

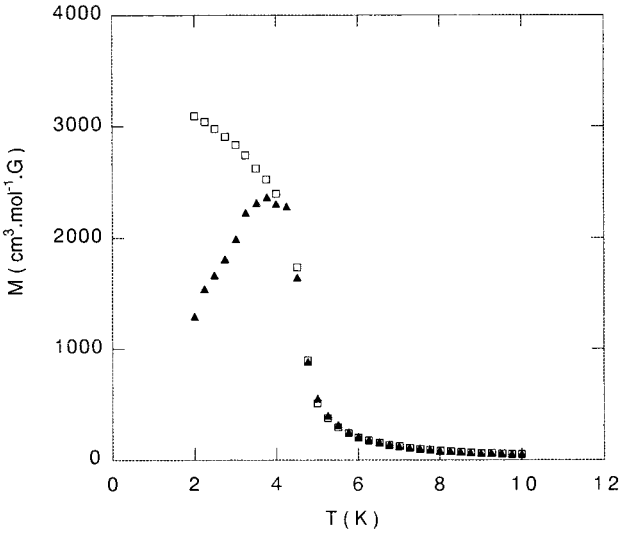

Figure 5. Temperature dependence of the magnetization (M) of $[(dmaph)PPh_3][Mn^{II}Cr^{III}(ox)_3]$: field-cooled magnetization (FCM) at 50 G (white square) and zero field-cooled magnetization (ZFCM) (black triangle).

Table 3. Magnetic Data for $[(dmaph)Pph_3][Mn^{II}Cr^{III}(ox)_3]$, Compared to Those of Previously Reported $A[Mn^{II}Cr^{III}(ox)_3]$ Ferromagnets

A^+	$\chi_M \times T$ ($cm^3\ mol^{-1}$)[a]	θ (K)	T_C (K)
$[(dmaph)PPh_3]^+$	6.0	8.7	4.5
$[mhs]^{+b}$	6.2	7.7	5.7
$[NBu_4]^{+c}$		7.2	6.0
$[PPh_4]^{+d}$		10.5	5.9

[a] Room temperature $\chi_M \times T$ value. [b] 4-Methoxy-*N*-heptylstilbazolium (ref 10). [c] Reference 31. [d] Reference 23.

Magnetic Properties. The temperature dependence of $\chi_M \times T$ and $1/\chi_M$ (χ_M being the molar magnetic susceptibility and T the temperature) are shown in Figure 4 for $[(dmaph)PPh_3][Mn^{II}Cr^{III}(ox)_3]$, while the molar magnetization (M) in the low-temperature regions is shown in Figure 5. The room temperature $\chi_M \times T$ value (6.0 $cm^3\ mol^{-1}\ K$) corresponds roughly to the sum of the uncoupled Cr^{III} (1.88) and Mn^{II} (4.38) value. As for other reported $A[MnCr(ox)_3]$'s (where A^+ is a bulky monocation), the magnetic properties of $[(dmaph)PPh_3][MnCr(ox)_3]$ are mainly characterized by ferromagnetic interactions between Cr^{3+} and Mn^{2+} and a long range ferromagnetic ordering at low temperature. Given the two-dimensional crystal structure, the intraplane interaction through the oxalate bridge is expected to be the strongest. The long-range ferromagnetic ordering observed at low temperature probably results from either a small interplane interaction (most likely dipolar interaction given the interlayer separation) or a small magnetic anisotropy. The Weiss constant (θ), obtained from a linear fit of the $1/\chi_M$ plot over a temperature range of 50−300 K and the critical temperature T_C of $[(dmaph)PPh_3][Mn^{II}Cr^{III}(ox)_3]$ are given in Table 3 and compared to those previously reported for $(NBu_4)[Mn^{II}Cr^{III}(ox)_3]$ and $(PPh_4)[Mn^{II}Cr^{III}(ox)_3]$.[24,31] It is interesting to point out that although the crystal structures exhibit some differences, the main features of the magnetic properties are not significantly affected by the nature of A^+.

Molecular Hyperpolarizability of $[(dmaph)PPh_3]^+$ Cation. The optical absorption spectrum of $[(dmaph)PPh_3]Br$ recorded in methanol (Figure 6) reveals an intense band located at 306 nm ($\epsilon_{max} = 28\ 500\ M^{-1}\ cm^{-1}$), which can be compared with the INDO data gathered in Table 4. The calculated spectrum is dominated by an intense transition at 283 nm. The agree-

(31) Tamaki, H.; Zhong, Z. J.; Matsumoto, N.; Kida, S.; Koikawa, M.; Achiwa, N.; Hashimoto, Y.; Okawa, H. *J. Am. Chem. Soc.* **1992**, *114*, 6974.

Table 4. Experimental and ZINDO-Computed Data for the Low-Lying Optical Transitions of $[(dmaph)PPh_3]^+$

	λ_{max} in nm		oscillator strength				
transitions	calc	exp	calc	exp[a]	$\Delta\mu$ in D	state %[b]	composition of CI expansion[c]
$1 \rightarrow 2$	294		0.14		12	10	$-0.543\chi_{69\rightarrow77} - 0.524\chi_{69\rightarrow72} + 0.337\chi_{69\rightarrow74}$
$1 \rightarrow 3$	283	305	0.58	0.50	16	55	$0.564\chi_{69\rightarrow70} - 0.481\chi_{69\rightarrow72} - 0.372\chi_{69\rightarrow77}$

[a] Reference 32. [b] Contribution of the ith transition to the β_{2level} (state % $= \beta_{g\rightarrow e(i)}/\sum_{j=1}^{j=100} \beta_{g\rightarrow e(j)}$). [c] Orbital 69 is the HOMO and orbital 70 the LUMO for $[(dmaph)PPh_3]^+$.

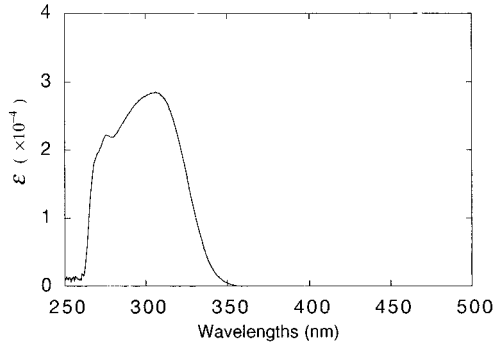

Figure 6. Optical spectrum of $[(dmaph)PPh_3]Br$ in MeOH.

ment in the relative energies and intensities between the calculation and the experimental data is found satisfactory.

It has long been recognized that the second-order NLO response of "push−pull" polyene derivatives is related to intense low-lying electronic transitions having charge-transfer character according to the "two-level" quantum desciption of the quadratic hyperpolarizability:[33]

$$\beta_{XXX} \propto \Delta\mu \times f/E^3$$

where E is the energy of the transition, f is its oscillator strength, and $\Delta\mu$ is the difference between the ground- and excited-state dipole moment. The β value calculated at 1.064 μm reaches 30.6×10^{-30} cm^5 esu^{-1}, a sizable value comparable to the 30×10^{-30} cm^5 esu^{-1} obtained for the *p*-nitroaniline, either theoretically[34] or experimentally.[33a] At first, this result seems surprising, as the strong acceptor ($-NO_2$) of the *p*-nitroaniline does not seem to find its counterpart in $[(dmaph)PPh_3]^+$. Table 4 reveals that the $1 \rightarrow 3$ transition is responsible for 55% of the NLO effect in $[(dmaph)PPh_3]^+$. Therefore, understanding the charge-transfer process associated with this transition provides a qualitative understanding of β. The composition of the configuration interaction indicates that excitations $\chi_{69\rightarrow70}$ and $\chi_{69\rightarrow72}$ contribute 32 and 23%, respectively, to the effect. Orbitals 69 (HOMO), 70 (LUMO), and 72 are drawn in Figure 7. It can be observed that most of the electron density of the HOMO (97%) is located on the dimethylaminophenyl fragment, in full agreement with the presence of a strong donor substituent on the ring. Interestingly, 84% of the electron density of orbital 70 is shared by the three phenyl substituents (89% for orbital 72), which provides an enhancement of the charge delocalization through the *d* orbital core of the phosphorus and hence

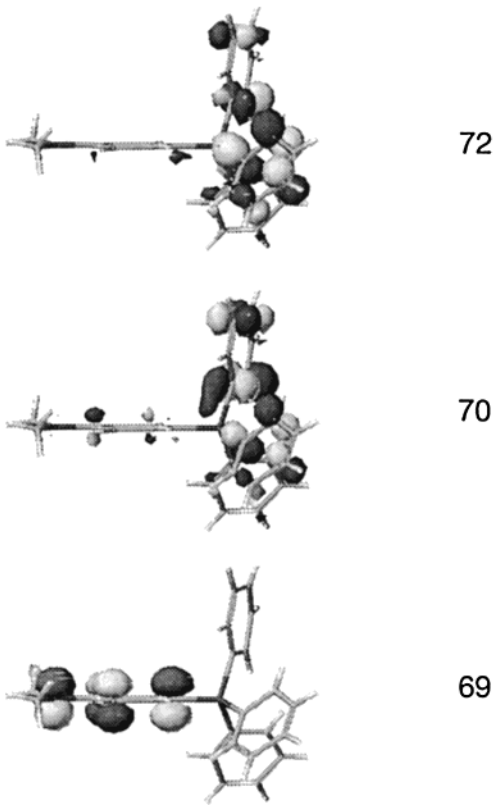

Figure 7. Main molecular orbitals involved in the NLO response of $[(dmaph)PPh_3]^+$.

a possibility for sizable NLO response in the material. Nevertheless, $[(dmaph)PPh_3][Mn^{II}Cr^{III}(ox)_3]$ exhibits vanishing bulk NLO properties as a result of the deliterious effect of a pseudo-centrosymmetric crystal environment. By contrast, powder SHG efficiencies equal to 1 and 4 times that of urea at 1.064 and 1.907 μm, respectively, were measured for the parent $[(dmaph)PPh_3]Br$, which probably crystallizes in a more favorable solid-state environment.

The successful introduction of NLO cations into $[Mn_{2-x}P_2S_6]^{2x-}$ or $[Mn^{II}Cr^{III}(ox)_3]^-$ anionic magnetic networks raises the possibility that the NLO response will be affected by a magnetic transition of the host lattice. The concept of NLO switching is attracting increasing interest, and has recently been reviewed.[35] Up to now, most strategies for switching of NLO materials have been based on a β modulation by mean of isomerization[36,37] or redox/proton transfer.[38−40] On the

(32) $f = 4.315 \times 10^{-9} \int\epsilon\, d\nu$. Orchin, M.; Jaffé, H. H. *Symmetry Orbitals, and Spectra*; John Wiley: New York, 1971; p 204.
(33) (a) Oudar, J. L.; Chemla, J. *J. Chem. Phys.* **1977**, *66*, 2664. (b) Oudar, J. L. *J. Chem. Phys.* **1977**, *67*, 446.
(34) Morrel, J. A.; Albrecht, A. C. *Chem. Phys. Lett.* **1979**, *64*, 46.
(35) Coe, B. J. *Chem. Eur. J.* **1999**, *5*, 2464.
(36) Clays, K.; Hendrickx, E.; Triest, M.; Verbiest, T.; Persoons, A.; Dehu, C.; Brédas, J.-L. *Science* **1993**, *262*, 1419.
(37) Loucif-Saïbi, R.; Nakatani, K.; Delaire, J. A.; Dumont, M.; Sekkat, Z. *Chem. Mater.* **1993**, *5*, 229.
(38) Coe, B. J.; Houbrechts, S.; Asselberghs, I.; Persoons, A. *Angew. Chem., Int. Ed.* **1999**, *38*, 366.
(39) Nakatani, K.; Delaire, J. A. *Chem. Mater.* **1997**, *9*, 2682.

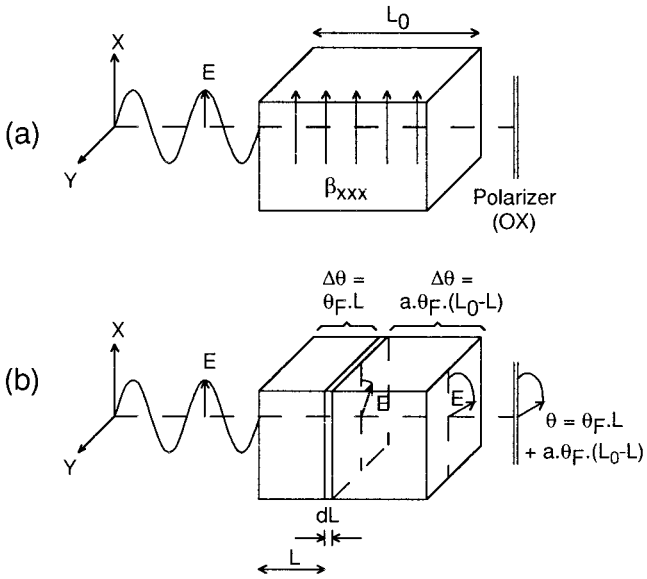

Figure 8. Experimental setup assumed in the calculation of the effect of a magnetic transition on the NLO properties of an idealized one-dimensional material. The magnetization is along OZ.

other hand, the propagation of a laser beam could be affected while propagating through a magnetic material. This behavior, which does not affect β, could modulate the SHG signal. This possibility is envisioned in the next section on the basis of the structural data available.

Potential Effect of the Faraday Rotation on the SHG Response. The most familiar of the magneto-optical effects is the rotation of the axis of linearly polarized light that occurs upon passage through a magnetized material. This is commonly called the Faraday rotation.[41] For a paramagnetic material, the magnetic rotation (θ) is expressed as

$$\theta = VBl$$

in which B is the applied magnetic field, l the thickness of the sample, and V the Verdet constant. Large V values, in the range $10°-100°$ cm^{-1} T^{-1}, can lead to sizable effects for high field intensity (>10 T) and particle size (>10 μm) in a range where the materials have to be phase matchable if NLO applications have to be considered. By contrast, θ no longer depends on the external magnetic field but on the internal magnetization in the case of propagation through a permanent magnet. The specific rotations (θ_F) of magnetic materials scale over many decades and can reach as high as 10^5-10^6 deg cm^{-1},[42,43] which leads to large rotations even upon transmission through thicknesses around 1 μm.

It is interesting to try to quantify the modifications that might occur in the quadratic NLO response for a hybrid material that undergoes a transition from a paramagnetic state to a ferromagnetic one. In the idealized situation depicted in Figure 8a, a laser beam is polarized along OX ($E_0 = E_X$). For the sake of simplification, all chromophores are parallel and possess

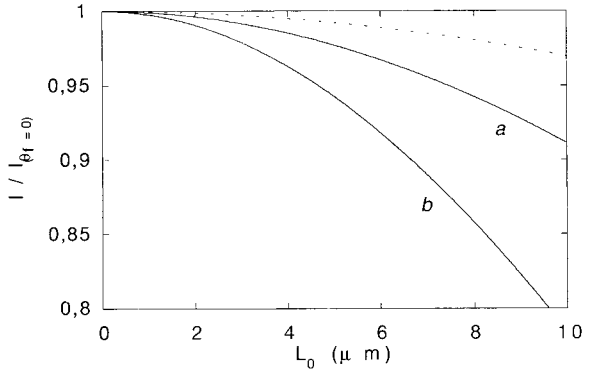

Figure 9. Modulation of the SHG light intensity induced by the Faraday effect ($I/I_{\theta_F=0}$) with $\theta_F = 10^{-4}$ deg cm^{-1}, for $\theta_{F(2\omega)} = 2\theta_{F(\omega)}$ (*a*) and $\theta_{F(2\omega)} = 4\theta_{F(\omega)}$, (b). The effect at ω frequency is given as a reference (dotted line).

a β tensor with a single nonvanishing component (β_{XXX}) in such a way that the 2ω polarization in a single molecule ($p_{2\omega}$) is equal to $\beta_{XXX}(E_0)^2$. As long as the thickness (L_0) of the crystal is small relative to the coherence length, velocity dispersions between ω and 2ω frequencies are negligible, and the macroscopic 2ω polarization along OX ($(P_{2\omega})_X$) will be proportionnal to $\beta_{XXX}(E_0)^2L_0$, in the nonmagnetic (or paramagnetic) state, where the Faraday rotation can be neglected. After magnetic ordering, with the magnetization directed along OZ, the contribution of an element of thickness dL (Figure 8b) to $(P_{2\omega})_X$ becomes proportional to

$$\mathrm{d}(P_{2\omega})_X \propto \beta E^2\,\mathrm{d}L = \beta_{XXX}(E_0)^2\cos^2(\theta_F L)\,\mathrm{d}L$$

The SHG light is subjected to further Faraday rotation, which is known to be frequency dependent ($(\theta_F)_{2\omega} = (a\theta_F)_\omega$, with $a > 1$). This leads to

$$\mathrm{d}(P_{2\omega})_X \propto \beta_{XXX}(E_0)^2\cos^2(\theta_F L)\cos(\theta_F L + a\theta_F(L_0 - L))\,\mathrm{d}L$$

The integration over the entire length of the crystal gives

$$(P_{2\omega})_X = (1/2)\beta_{XXX}(E_0)^2\left(\int_0^{L_0}\cos[(1-a)\theta_F L + a\theta_F L_0]\,\mathrm{d}L + \int_0^{L_0}\cos(2\theta_F L)\cos[(1-a)\theta_F L + a\theta_F L_0]\,\mathrm{d}L\right)$$

and finally[44]

$$(P_{2\omega})_X = (1/2)\beta_{XXX}(E_0)^2\left(\frac{\sin(\theta_F L_0) - \sin(a\theta_F L_0)}{(1-a)\theta_F} + \frac{\sin(\theta_F L_0) + \sin(a\theta_F L_0)}{2(1+a)\theta_F} + \frac{\sin(3\theta_F L_0) - \sin(a\theta_F L_0)}{2(3-a)\theta_F}\right)$$

The modulation of the light intensity (I) induced by the Faraday effect, which is proportional to the square of the above expression ($I \propto (P_{2\omega})^2$), has been calculated for $\theta_F = 10^4$ deg cm^{-1} in Figure 9, for $a = 2$ and 4. It appears that the effect is much greater on the SHG

(40) Evans, C. C.; Bagieu Beucher, M.; Masse, R.; Nicoud, J.-F. *Chem. Mater.* **1998**, *10*, 847.
(41) Dillon, J. F. *J. Appl. Phys.* **1968**, *39*, 922.
(42) Breuer, W.; Jaumann, J.; Smith, D. O. *Z. Phys.* **1963**, *173*, 117.
(43) Hansen, P.; Clausen, C.; Much, G.; Rosenkranz, M.; Witter, K. *J. Appl. Phys.* **1989**, *66*, 756.

(44) For $a = 1$, $(S^{2\omega})_X = (1/2)\beta_{XXX}(E_0)^2\cos(\theta_F L_0)(L_0 + (\sin(2\theta_F L_0)/(2\theta_F))$, and for $a = 3$, $(S^{2\omega})_X = (1/2)\beta_{XXX}(E_0)^2((\sin(\theta_F L_0) - \sin(3\theta_F L_0)/(-2\theta_F) + \cos(3\theta_F L_0)(\sin(4\theta_F L_0)/(8\theta_F)) + (L_0/2) - ((\sin(3\theta_F L_0)(\cos^2(2\theta_F L_0) - 1))/(4\theta_F))$.

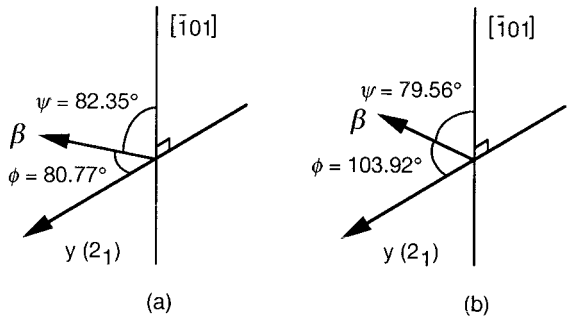

Figure 10. Orientation of β versus the easy axis of magnetization [$\bar{1}$01] and the 2-fold axis of the crystal for cation **1** (a) and **2** (b).

intensity than on the ω counterpart. This observation suggests that a sizable switch in the NLO response could be envisionned in such molecular devices upon magnetic ordering by means of the Faraday effect.

Before considering this possibility, several issues must be adressed related to the orientation of β in the crystal. First, the Faraday effect requires that the laser beam propagates along the magnetization axis ($M = M_Z$ in Figure 8). Therefore, optimizing the NLO response implies that β is orthogonal with respect to the magnetization. In the case of layered magnets such as $[Mn_{2-x}P_2S_6]^{2x-}$ and $[Mn^{II}Cr^{III}(ox)_3]^-$, previously reported studies have revealed that the magnetization is directed perpendicular to the anionic layers (easy axis of magnetization),[45,46] which corresponds to the [$\bar{1}$01] direction in the present crystal structure. The angle (ψ) between the vectorial β calculated for both $[(dmaph)PPh_3]^+$ cations and the magnetization axis is drawn in Figure 10. The value is equal to 82.35° and 79.56° for cations **1** and **2**, respectively, which would indicate a nearly optimized orientation. In the case of **1** (and other related intercalated derivatives), although no crystal structure is available, the interlamellar distance strongly suggests that the charge-transfer axis of $DAMS^+$ cations (and hence the hyperpolarizability) is roughly parallel to the $[Mn_{2-x}P_2S_6]^{2x-}$ slabs (Scheme 1)[47] and therefore perpendicular to the magnetization axis. Therefore, nearly optimized β orientations seem to be a trend in all these layered solids. On the other hand, it is well-known that the chromophores must be engineered in non-centrosymmetric environments if β is to contribute to an observable bulk susceptibility ($\chi^{(2)}$). In the case of $[(dmaph)PPh_3][Mn^{II}Cr^{III}(ox)_3]$, which crystallizes in space group $P2_1$, the relationships between β and $\chi^{(2)}$ (components d_{IJK} in crystalline frame) leads to the following relations:[48,49]

$$d_{YXX} = N \sum_i \beta_i \cos \phi_i \sin^2 \phi_i$$

$$d_{YYY} = N \sum_i \beta_i \cos^3 \phi_i$$

Scheme 2

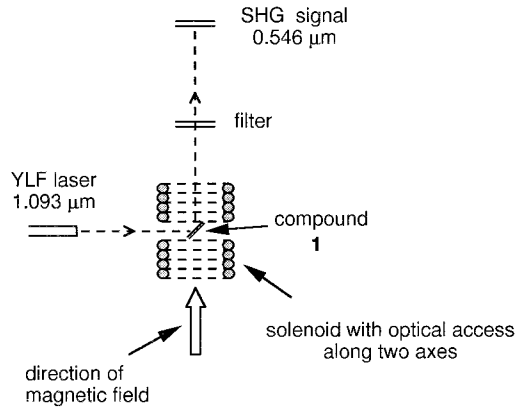

All other components of the tensor are weak (ϕ is defined as the angle between β and the 2-fold axis OY of the crystal, and the summation is performed over the four cations in the unit cell).

In the present case, ϕ is equal to 80.77° and 103.92° for cations **1** and **2**, respectively (Figure 10). The larger angular factors weighting β are 0.156 (cation **1**) and −0.227 (cation **2**) for d_{YXX}, which are modest but nonzero values. However, the opposite signs lead to almost vanishing NLO properties after summations over the crystal cell, in agreement with the zero SHG recorded for $[(dmaph)PPh_3][Mn^{II}Cr^{III}(ox)_3]$. To further analyze the possibilities provided by this $P2_1$ structure, it is worth pointing out that rotations of β around the [$\bar{1}$01] direction could modulate and finally optimize ϕ without changing the ψ value. The situation with $\phi = 54.74°$, which optimizes d_{YXX}, has been reported as being the most favorable among any space groups.[49] Therefore, this class of NLO chromophores containing lamellar magnets is compatible for both optimized SHG efficiency (ϕ around 54°) and optimized NLO modulation by Faraday effect (ψ around 90°).

Reliable measurements and analysis of the NLO modulation occurring upon magnetic ordering in such layered magnets require compounds with observable bulk NLO properties available as large single crystals to prevent any motion of the grains due to undesirable magnetic effects. Moreover, this would also allow the optimization of the orientation of the laser beam with respect to the chromophores and hence the quantification of the interplay between the properties. None of the present $[(dmaph)PPh_3][Mn^{II}Cr^{III}(ox)_3]$, $Mn_{0.86}P_2S_6$-$(DAMS)_{0.28}$ (**1**), and $(MHS)[Mn^{II}Cr^{III}(ox)_3]$ (**2**) magnets fulfill all these requirements. However, $Mn_{0.86}P_2S_6$-$(DAMS)_{0.28}$ offers the most suitable sample for a measurement, with a large SHG efficiency and a magnetic ordering occurring at rather high temperature (40 K).

A test has been performed in an optical cryostat on an uncalibrated microcrystalline sample of compound **1** put in the center of a superconducting solenoid (Scheme 2). Because of strong absorption at the 2ω frequency, the SHG intensity had to be measured by reflection.[50] It was observed that a field of about 0.5 T causes a decrease of the SHG intensity of ≈10% as the

(45) Pellaux, R.; Schmalle, H. W.; Huber, R.; Fischer, P.; Hauss, T.; Ouladdiaf, B.; Decurtins, S. *Inorg. Chem.* **1997**, *36*, 2301.
(46) Iijima, S.; Mizutani, F. *Mol. Cryst. Liq. Cryst.* **1999**, *335*, 143.
(47) Lacroix, P. G.; Veret Lemarinier, A. V.; Clément, R.; Nakatani, K.; Delaire, J. A. *J. Mater. Chem.* **1993**, *3*, 499.
(48) Oudar, J. L.; Zyss, J. *Phys. Rev. A* **1982**, *26*, 2016.
(49) Zyss, J.; Nicoud, J. F.; Coquillay, M. *J. Chem. Phys.* **1984**, *81*, 4160.

(50) For the use of SHG measurement by reflection, see for example: (a) Shen, Y. R. *Nature* **1989**, *337*, 519. (b) Gillberg, G.; Keosian, R.; Pruksarnukul, J. L.; Lupo, D. W. *Mol. Eng.* **1991**, *1*, 191. (c) Meech, S. R.; Yoshihara, K. *Chem. Phys. Lett.* **1989**, *154*, 20.

temperature is lowered below T_C (to 10 K).[51] In such an experiment, the question of possible grain motion has to be considered, even if the sample is a microcrystalline powder very tighly pressed between glass plates. To prevent this undesirable effect (or reduce its magnitude as much as possible), the selected field ($H = 0.5$ T) is chosen at the begining of the plateau regime, after the initial sharp increase on the isothermal magnetization curve $M = f(H)$.[9] Doing so, it is ensured that the magnetic ordering undoubtly takes place in the material, while the magnetic strength is minimized. In addition, it is worth pointing out that, under these conditions, the resulting magnetization in $Mn_{0.86}P_2S_6$-$(DAMS)_{0.28}$ is equal to 800 emu/mol Mn. This is equal to $^1/_{30}$th of the theoretical value obtained if all of the spin of the Mn^{II} was aligned and therefore corresponds to a very weak magnetization. Consequently, the possiblilty for powder alignment along the field is probably very limited and may likely be unsufficient to account for a 10% modulation of the SHG signal.

Although the above observation is suggestive that the SHG behavior may be subjected to modulation while occurring in a magnetized medium, any attempt to further quantify this behavior experimentaly necessarily requires the growth of single crystals of **1**. Unfortunatly, such single crystals cannot be obtained for reasons related to the intercalated process used in the synthetic procedure. This limitation should stimulate the investigation of the alternative $[Mn^{II}Cr^{III}(ox)_3]^-$-based materials as a more promising family for future investigations.

Conclusion

$[(dmaph)PPh_3][Mn^{II}Cr^{III}(ox)_3]$ is a new molecular-based ferromagnet with a critical temperature of $T_C =$ 4.5 K. The structure is made of anionic magnetic layers with $[(dmaph)PPh_3]^+$ cations inserted in between. INDO calculations reveal that the molecular NLO response of the cations is close to that of the well-known *p*-nitroaniline, which should ensure a SHG signal, in relation to a non-centrosymmetric space group ($P2_1$). Even if no bulk properties are evidenced, because of pseudo-centrosymmetric packing of the cations in $[(dmaph)PPh_3][Mn^{II}Cr^{III}(ox)_3]$, a theoretical investigation reveals that the symmetries of this magnet are compatible with both optimized NLO properties and optimized NLO modulation by the Faraday effect. Up to now, various non-centrosymmetric $[Mn_{2-x}P_2S_6]^{2x-}$- and $[Mn^{II}Cr^{III}(ox)_3]^-$-layered-based magnets have been reported in which NLO cations can be inserted. The present report has provided a set of theoretical, structural, and experimental features that tend to demonstrate the potential capabilities of these structures for magnetically induced NLO modulation. Obtaining large single crystals of these hybrid magnets is undoubtly the next step in this research program to overpass the present bottlenecks toward the full understanding and quantification of the potential capabilities of these multifunctional materials.

Acknowledgment. The authors thank Prof. R. Clement (LCI-Orsay), Prof. A. H. Francis (University of Michigan), and Dr. J. C. Daran (LCC-Toulouse) for helpful discussions.

Supporting Information Available: Atomic coordinates and equivalent isotropic displacement parameters, selected bond lengths and angles, anisotropic displacement parameters, and hydrogen coordinates and isotropic displacement parameters for yumn2 (PDF). This material is available free of charge via the Internet at http://pubs.acs.org.

CM001177V

(51) Francis, A. H., unpublished observation.